Journal of the Ceramic Society of Japan 117 [3] 221-227 2009 **Special Article: Review**

Calcite mesocrystals: a very effective block polyelectrolyte for crystal "Morphing"

Tongxin WANG, Andreas VERCH, Hans G. BÖRNER, Helmut CÖLFEN and Markus ANTONIETTI

Max-Planck-Institute of Colloids and Interfaces, Department of Colloid Chemistry, Research Campus Golm, D−14424 Potsdam, Germany

A family of calcite nanocrystal superstructures with unusual morphology were obtained from crystallization of calcite by the CO_2 gas diffusion technique in the presence of a bioinspired double hydrophilic block copolymer, polyethyleneglycol-block-poly (L-aspartic acid). From the typical calcite rhombohedra as a starting situation, the morphology can be systematically varied via various unusual porous mesocrystal morphologies to hemispheres composed of fine calcite triangles. The formation of mesocrystals is starting at a polymer concentration of only 10^{-3} g/L and shows two remarkable results: (a) the reported bio-inspired block copolymer is the so far most active polymer for mesocrystal formation reported to our knowledge, and (b) the data prove that nucleation promoters exist, which can form nanocrystals for mesocrystal formation even without enhanced colloidal stabilization. This gives mesocrystal formation a much broader operation range than previously assumed.

Key-words : Mesocrystal, Double hydrophilic block copolymer, Non-classical crystallization, Morphogenesis, Calcite

[Received December 1, 2008]

1. Introduction

Bottom up approaches for the self organization of matter are a cornerstone of nanotechnology and of great importance for future materials science. Especially for crystalline systems with their structural anisotropy, it is a challenge to structure nanoparticles in a way that the nanoparticles are mutually oriented or even orient into a mutual crystallographic register. Since the key observation of Penn and Banfield on crystal growth by oriented aggregation of nanoparticles,[1),2)] this mechanism was found for a steadily increasing number of systems as recently reviewed.[3)] As further non classical crystallization mechanism, the formation of mesocrystals was also discovered.[4),5)] Mesocrystal is an abbreviation for "mesoscopically structured crystal" meaning a crystalline superstructure with mutual orientation of its nanoparticle building units.[5)] Mesocrystals with perfect 3D orientation are of special interest, since they scatter/diffract like a single crystal but are composed of nanoparticle building units offering to combine single crystal properties with those of typical colloids like high internal surfaces etc. A continuous transition in building unit particle size to molecules on the one hand and of decreasing mutual order of the nanoparticle subunits on the other, places mesocrystals as structural intermediate between a classical single crystal composed of atoms/ions/molecules and a polycrystal without any mutual order between its nanoparticle subunits.[6)] This intermediate structure of mesocrystals between single crystal and polycrystal was very recently also found for Ag mesocrystals.[7)] Mesocrystals are usually not stable against crystallographic fusion of their nanoparticle subunits to a single crystal, if their nanoparticle subunits are in crystallographic register, since the subunits are aligned and the system can win a substantial amount of energy by elimination of these internal surfaces.[1),2)] This could indeed be shown experimentally.[8),9)] Mesocrystals have meanwhile been reported for a number of different systems as reviewed in[3)–5),10)–12)] including maghemite,[13)] vaterite,[14),15)] calcite,[16)–18)] K_2SO_4–PAA,[19)] $BaSO_4$,[20)] alanine,[21),22)] CdS,[23)] $CoPt_3$[24)] and also a number of further materials with specific functions, which are improved by the mesocrystal structure, including Ag,[7)] β–$Ni(OH)_2$,[25)] Ibuprofen,[26)] $PbTiO_3$,[27)] ZnO,[28),29)] $BiVO_4$[30)] or TiO_2[31)] to name just a few of the very recent examples.

Interestingly, Nature also applies this non-classical crystallization concept and several Biominerals recently turned out to be mesocrystals like sea urchin spines,[32)–34)] sponge spicules,[35)] foraminifera,[33)] nacre,[33),36)–40)] calcite prisms in mussel shells,[41)] corals[33)] or egg shells.[33)] Such a structure formation is clearly different to the idealized thermodynamic viewpoint of the classical crystallization process, which has been pioneered early last century by Wulff .[42)]

Despite the rapidly increasing number of observations of mesocrystals, relatively little is yet known about their formation mechanism. In a series of papers[43)–45)] we demonstrated that addition of a simple polyelectrolyte as poly (styrene sulfonate) can modify the crystal growth of calcium carbonate in a manifold fashion leading to nanocrystal superstructures with astonishing complexity. The remarkable change from the typical single crystal calcite rhombohedron with (104) faces to mesocrystals presenting their unusual {001} faces with additional rounded edges was outlined. The results implied that a dipole along the c-axis drove the nanoparticle assembly.

In these papers, we also discussed the role of the polymer which can interfere with crystallization of an ionic crystal in multiple ways. For instance, it binds ions by electrostatic forces,[46),47)] thus blocking the ionic growth path, but also providing a template for nucleation. Also, intermediate structures, such as amorphous precursor structures can be colloidally stabilized by a surface layer of polymers. Once these isotropic particles crystallize, the additives can adsorb face selectively and can therefore alter the shape of the developing nanocrystals.[48)] In addition, the bound polymers can induce a directed aggregation through a change of interaction potentials, which can be highly directional and anisotropic.[43),44)] Usually, the added polymers have one or more than one, if not all roles of that list.

It is the task of the present paper to extend these primary observations by changing from the very simple polyelectrolyte to a double hydrophilic block copolymer (DHBC, see. Ref.49) which is made and optimized to interact with crystal growth and to temporarily stabilize primary nanoparticles as building units for further self organization. We choose a water soluble stabilizing poly (ethylene oxide) PEO block and a uniform polyaspartate block as interacting block, made by SPPS (solid phase peptide synthesis). Such a polymer is a model for the Asp-rich proteins, which consist of a high amount of aspartic acid and hydrophilic units and which were recently discovered as active molecules for crystallization control in Biomineralization.[50),51)] DHBC's consisting of PEO and an interacting peptide block already proved to be efficient crystallization modifiers for $CaCO_3$[52)] and D, L-alanine.[53)] With this advanced and defined polymer design, we hope to raise additional evidence how and at which crystallization stage different polymers interfere with the crystallization and aggregation process and in which further modes mesocrystallization can occur.

2. Experimental

Polymer synthesis: N-α-Fmoc protected aspartic acid derivative (Fmoc-Asp(*t*Bu) OH), 2-(1H-benzotriazole-1-yl)-1, 1, 3, 3-tetramethyluronium hexafluorophosphate (HBTU), *N*-methyl-2-pyrrolidone (NMP, 99.9+ %, peptide synthesis grade) were used as received from IRIS Biotech GmbH, Germany. Dichloromethane (DCM, IRIS Biotech GmbH (peptide grade)) was distilled from CaH_2 prior to use. TentaGel PAP resin (PEO attached peptide resin, loading: 0.21 mmol/g; M_n = 3200 g/mol, M_w/M_n = 1.05) was obtained from Rapp Polymere GmbH (Tübingen, Germany).

The crystal growth modifier, a peptide-polymer conjugate was synthesized by applying a fully-automated, inverse conjugation strategy.[54)] The bioconjugate combined a poly (ethylene oxide) block (PEO) of M_n = 3200 g/mol with a monodisperse, sequence controlled polypeptide segment of twenty repeats of L-aspartic acid ((L-Asp)$_{20}$). The PEO-*b*-(L-Asp)$_{20}$ (PEO–D_{20}) (***I***)) was synthesized via sequential assembly of Fmoc-Asp(*t*Bu) OH monomers on a PEO preloaded polystyrene resin (PAP), using solid-phase supported peptide synthesis protocols (SPPS).[55)] The coupling of the Fmoc-Asp(*t*Bu) OH building blocks was facilitated by HBTU in NMP and Fmoc removal was achieved with piperidine as described previously. **I** was liberated by 6 h treatment with 99.8% trifluoroacetic acid (TFA) and 0.2% trimethylsilyl bromide. The liberated peptide-conjugate was isolated by precipitation in diethyl ether, centrifugation and dialysis (MWCO ≈ 1000 g/mol) against Millipore water, followed by lyophilization from water. The structural identity of the product was confirmed by ^{1}H–NMR. Analysis of **I**: ^{1}H–NMR (D_2O): δ = 2.63 (m, ~40 H, $C^{\beta}\underline{H}_2$, Asp), 3.55 (*m*, 280 H, –O–C$\underline{H}_2$–C$\underline{H}_2$–O–, PEO), 4.60 (*m*, ~20 H, –C$^{\alpha}$H–, Asp) ppm.

Crystallization of $CaCO_3$: $CaCl_2 \cdot 2H_2O$ (Fluka, ≥ 99%) and $(NH_4)_2CO_3$ (Fluka, ≥ 30% NH_3 basis) were used without further purification. Double distilled water was used for the preparation of the crystallization solutions. The mineralisation was performed by a slow CO_2 gas diffusion technique as described in our previous papers.[43),44)] To investigate the effect of added polymer, crystallizations were performed in the presence of different concentrations of polymer and $CaCl_2$ in glass bottles with glass slides, which were put into the same closed desiccator at room temperature. All glassware including glass bottles and small pieces of glass substrates were cleaned as follows: firstly sonicated in ethanol, then rinsed with distilled water, further soaked with a H_2O–HNO_3 (65%)–H_2O_2 (1:1:1, v/v/v) solution, then rinsed with doubly distilled H_2O, and finally dried at room temperature.

A stock solution of $CaCl_2$ (10 mM) was freshly prepared in boiled doubly distilled water and bubbled with N_2 overnight. 5 mL of the solutions at different concentration of PEO–D_{20} (1.0, 0.75, 0.5, 10^{-1}, 10^{-2}, 10^{-3} g/L) were prepared from the above $CaCl_2$ solution under vigorous stirring. Then, the solution was equally separated into different glass bottles with a glass slide at the bottom (1 mL solution in each bottle) for further crystallization experiments. The bottles were covered with Parafilm and punched with three needle holes and placed in a larger desiccator (inner diameter 250 mm). Two small glass bottles (10 mL) with crushed ammonium carbonate were also covered with Parafilm, punched with three needle holes, and placed at the bottom of the desiccator. At different times, the bottles were taken out from the desiccator and the Parafilm was removed. After the solution was taken out, the glass slides with the crystals were rinsed with distilled water and examined by optical microscopy. After drying at room temperature, the crystals were examined by SEM and other techniques.

2.1 Analytical methods

Optical microscopy in solution and scanning electron microscopy (SEM) were applied to all samples. The use of the light microscopy technique is necessary in order to prove that the SEM micrographs show real structures instead of drying artefacts resulting from sample preparation. In addition, polarized light microscopy allows for the identification of the calcite (001) face, which is the only calcite face not showing double refraction. The SEM measurements were performed on a LEO 1550 – GEMINI REM. Light microscopy images were taken for samples in solution with an Olympus BX41 microscope connected with an Olympus Camedia 5060 colour camera. Powder X-ray diffraction (XRD) patterns were recorded on a PDS 120 diffractometer (Nonius GmbH, Solingen) with Cu Kα radiation. The surface cleavage of the crystal faces, the unit cell structure, and the modelling of morphologies were performed with the *Cerius*^{2} software (Accelrys).

2.2 Quantitative in-vitro crystallization assay

The utilized commercial Metrohm titration setup and experimental procedure are already described in detail elsewhere.[56)] In brief, calcium chloride solution (25 mmol/L) is dosed at a constant rate (0.01 mL/min) into carbonate buffer solution (pH = 9.75, 10 mmol/L, 25 mL), while the calcium potential is monitored and the pH-value is kept constant by means of titration utilizing 10 mmol/L NaOH. The experiment in absence of additives is the reference experiment. Experiments in presence of the PEO–D_{20} are carried out in the same carbonate buffer containing 0.01 g/L and 0.001 g/L polymer, respectively, which is directly weighed in.

3. Results and discussion

With the presented crystallization set-up and procedure, calcium carbonate crystallizes within only 1 day into well defined calcite rhombohedra (data not shown). The final recrystallization step towards the calcite single crystals most presumably takes place via ionic crystallization due the carbonate/bicarbonate equilibrium, in which the calcium ion concentration can be comparably high depending on the pH, which usually raises from below neutral to higher than pH 9 during the reaction.

Employing PEO–D_{20} as crystal growth modifier, a variety of

changes can be observed. Firstly, as compared to the previous experiments with polystyrenesulfonate,[43)–45)] the crystal morphology is already influenced at much lower polymer concentrations, exhibiting pronounced morphology changes. Already addition of traces (10^{-3} g/L) of PEO–D_{20} increases the crystallization speed, and the formed crystals are getting very homogeneous in morphology and size. This indicates that the polymer acts as a nucleation agent at low polymer concentration whereas it inhibits crystallization at higher concentrations.[57)]

Secondly, the morphology of the final calcite crystals is slightly altered, as exemplified in **Fig. 1**. The majority species are still rhombohedra, but they are heterogeneously nucleated from the glass slide and show rough surfaces with visible pores, channels and coarsened edges (Fig. 1(b)). The formation of porous crystals and rough surfaces as well as "etched" edges is a strong indication for the alteration of the crystallization mechanism from ionic growth to mesoscale assembly.[20)] It is quite informative to analyze a secondary structure (minority species in Fig. 1(c)), presumably nucleated from the continuous phase, which can indicate some common structural principles underlying the formation of both coexisting crystalline structures. These apple-shaped objects are obviously grown by aggregation of a large quantity of small nanoscopic intermediates. A closer look to those reveals that the tectonic units have a size of about 50 nm–300 nm and recrystallize towards poorly shaped calcium carbonate crystals with a significant portion of structural porosity. Reference experiments with the same block copolymer in the quantitative crystallization assay indicate that the precipitate is vaterite, while for heterogeneous nucleation on a glass surface, only calcite nucleates.

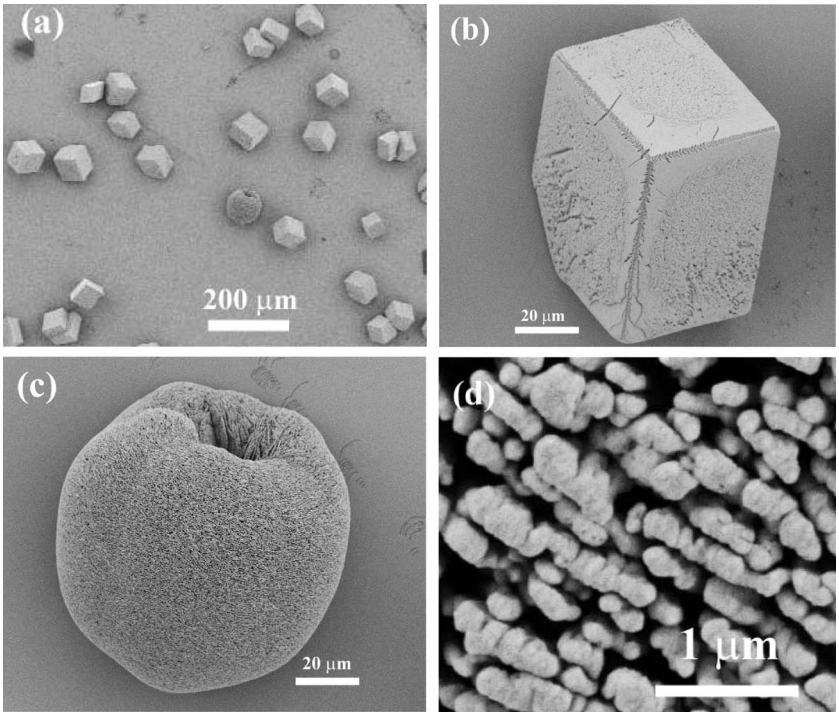

Fig. 1. High resolution SEM image of a calcite mesocrystal obtained from 1 mL of 10 mmol/L Ca^{2+} solution with 10^{-3} g/L PEO–D_{20}. Samples were obtained on a glass slip via gas diffusion experiment after one day; (a) overview image; (b) an enlarged image of the majority species. Note the formation of rough faces and coarsened edges; (c) an enlarged image of the minority species indicating possible precursor structures; (d) high resolution picture of the surface structure of (c) indicating that these mesocrystals are composed of 50–300 nm sized building blocks and possess a high structural porosity.

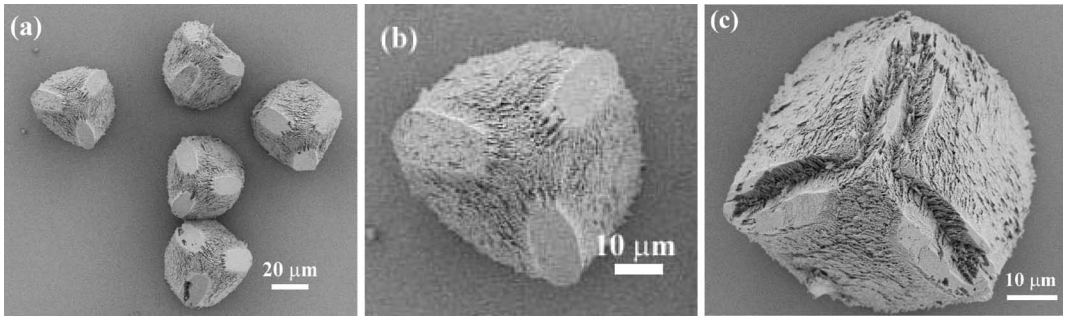

Fig. 2. High resolution SEM images of calcite mesocrystals obtained at 10 mmol/L Ca^{2+} solution with 10^{-2} g/L PEO-b-poly(L-Asp)$_{20}$. Samples were obtained on a glass slip via gas diffusion experiment after one day; (a) representative overview indicating the high uniformity of the species; (b), (c) magnification of different mesocrystals.

The unexpected important observation is that such porous scaffolds can be formed at extremely low polymer concentration (10^{-3} g/L). Such a low concentration is too low to allow for effective surface stabilization of the high surface area of particles with sizes of several tens of nm. Contrary to previous models of polymer activity,[58] the strong binding between free Ca^{2+} ions and polymer is not enough to significantly deplete the calcium ions in solution, as the polymer concentration corresponds to only 3.4×10^{-6} moles of carboxylate binding moiety. Therefore, the high efficiency of the present system can only be explained by its influence on pre-nucleation structures and the primary nucleated phase (see titration experiments below).

A concentration increase by a factor of 10 to still rather low 10^{-2} g/L results in a completely altered morphology of the crystal superstructures (**Fig. 2**).

The formerly observed rhombohedral shape of the heterogeneously nucleated crystals has been disintegrated and is only left as an engulfing hull, with three apparently planar faces still indicating the former {104} planes. The whole structure is subdivided into visible building blocks which have not fused to the final crystal. Previous studies show that under similar conditions calcite nucleates via the (001) plane from the glass substrate and is oriented with the *c*-axis towards the observer.[43),44)] This is also true here, as judged from the orientation of the three {104} faces. The edges which have been already suppressed at the lower concentration (10^{-3} g/L) turned into rough surfaces with oriented surface texture. The fact that also the three flat planes are composed of single nanocrystalline units, such as streets from cobblestones, is shown in Fig. 2(c) where such a mesocrystal has been partly broken up upon rapid drying. Due to the missing surface porosity, those flat surfaces can critically fail while drying, and one can recognize the homogeneity of the nanoparticular structure set-up in deeper parts of the particle which obviously extends throughout the microparticle. The ability to explode because of evaporation of water is also a clear proof for the porous character of the mesocrystal species.

A further indication for this mesoscale assembly is obtained from WAXS evaluations of the primary crystallite size in the final crystals, which reveal a primary calcite building unit of ca. 40–50 nm from Scherrer evaluation, regardless of the polymer and Ca^{2+} concentration as also found for the vaterite particles in the quantitative crystallization assay. This goes well with the size of the tectonic units observed in HRSEM. (Fig. 1, ca. 50 nm) These results clearly exclude structure densification by Ostwald ripening, which would lead to a single crystal without a pore system, and supports the electron microscopy evidence.

A closer examination of the early nucleation phases in presence of PEO–D_{20} was possible with the quantitative crystallization assay.[47),56)]

In **Fig. 3**, we show the time dependence of the effective ion product of calcium and carbonate ions in solution upon constant Ca^{2+} addition while the pH of the solution was kept constant at pH 9.75. It is seen that PEO–D_{20} in fact only slightly inhibits the nucleation. For a polymer content of 10^{-3} g/L there is no significant effect on the nucleation time detected while the nucleation event is delayed by ca. 25% when 10^{-2} g/L PEO–D_{20} is present in the carbonate buffer solution. More remarkable is the influence of the polymer on the species formed after nucleation. For the 10^{-3} g/L solution, the equilibrium solubility is lower than for the reference experiment without polymer, meaning that directly a crystalline phase is formed instead of amorphous intermediates. This is a clear signature of a nucleation agent with very high efficiency.

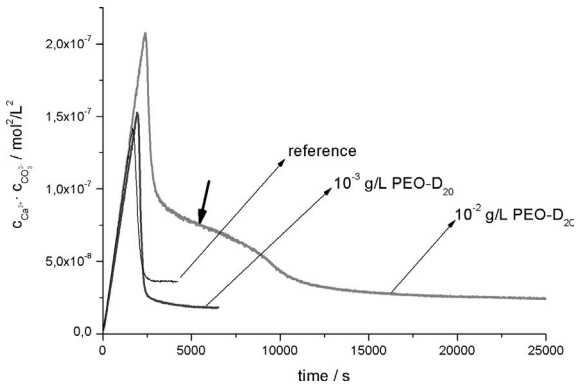

Fig. 3. Time development of the free ion product in absence of PEO–D_{20} (reference; dashed line), in presence of 10^{-3} g/L PEO–D_{20} (bold black line) and in presence of 10^{-2} g/L PEO–D_{20} (bold grey line). The bold arrow indicates the area of a nearly constant solubility product between the two nucleation events in presence of 10^{-2} g/L PEO–D_{20}. For further information see text.

For the 10^{-2} g/L solution, a more complex fingerprint in the titration curve is found. After the first sharp nucleation (after ca 3000 s) event the solubility product of the solution stays nearly constant on a level two times higher than the ACC formed in the reference experiment and in the same curve after a second step wise phase change (at around 8000 s). One reasonable rationalization for this very soluble intermediate phase is the formation of a polymer induced liquid precursor (PILP-phase), which can well be formed and temporarily stabilized by addition of polyaspartic acid.[59)] For concentrations of 10^{-2} g/L of the present polymer, this phase is only temporarily stable. The observation of such transient phase does not mean that no other crystalline nanoparticles are present in the crystallization assay, as the equilibrium ion concentration is only indicative for the most soluble species. We assume (from the final mesocrystal morphology) that in this concentration range the PEO–D_{20} polymer not only acts as a nucleation agent, but is also sufficiently concentrated to stabilize a PILP phase for some key time of reaction.

The existence of PILP droplets or amorphous particles in this reaction phase is also evidenced by optical polarized light microscopy (data not shown here). In the quantitative crystallization assay at 10^{-2} g/L PEO–D_{20}, 2400 s after nucleation only non-birefringent, amorphous particles are found, while another 2400 s later (still well before the second stepwise phase transition), bright spots of crystalline calcium carbonate are found. The number of crystallized particles then increases with time, but even 8000 s after nucleation, the majority of the particles is still amorphous.

Increasing the polymer concentration to 0.1 g/L at fixed Ca^{2+} concentration (10 mmol/L) leads again to the coexistence of two new, heterogeneously nucleated morphologies, which obviously differ by nucleation only. On the one hand, we observe another kind of rhombohedral particle where the overall morphology is now completely splitted into finer nanocrystallites (**Fig. 4**(a)). Again, those particles nucleate from flat glass via the (001) face. The symmetry of the object, as viewed from the c-axis orthogonal to the surface, indicates that the building blocks are carefully stacked to the mesocrystal where the outer shape is a product of energy minimization of the assembly process.

The other class of particles (Fig. 4(b)), nucleated predominantly at rough side positions of the cutted glass slide, is a rounded, more stretched morphology, which can not be repre-

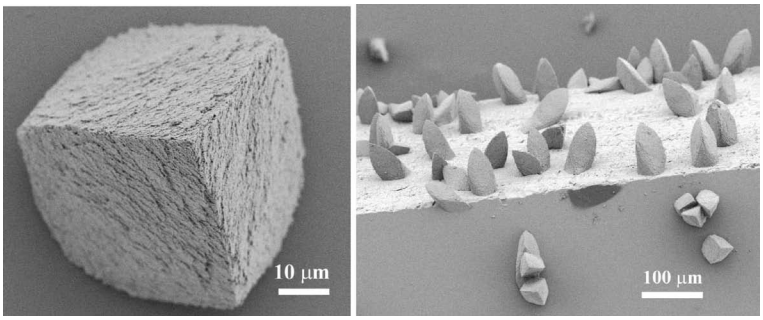

Fig. 4. High resolution SEM images of calcite mesocrystals obtained at 10 mmol/L Ca^{2+} solution with 0.1 g/L PEO-b-poly(L-Asp)$_{20}$. Samples were obtained on a glass slip via gas diffusion experiment after 1 d. The images show the two coexisting structures.

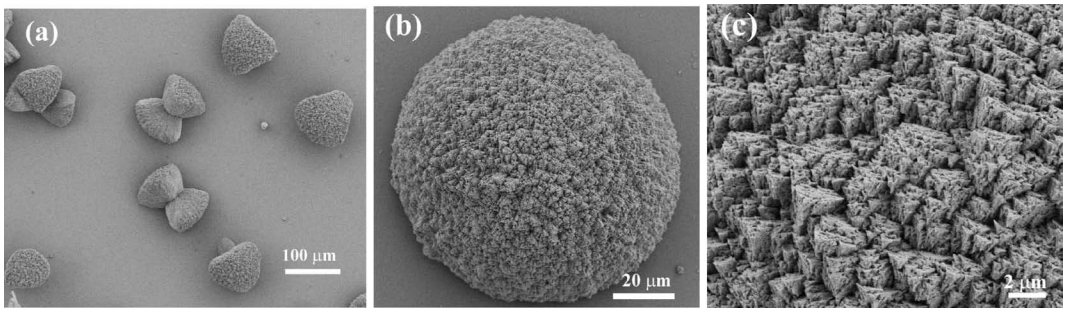

Fig. 5. Typical SEM images of calcite mesocrystals obtained on a glass slip by the gas diffusion reaction after 1 d at 10 mmol/L Ca^{2+} and [PEO-b- P(L-Asp)$_{20}$] = : (a) 0.5 g/L; (b) 0.75 g/L. (c) high magnification of the surface structure of (b).

sented by any of the classical crystalline calcite single crystal morphologies. This is regarded as evidence for the mesocrystal character of these structures, which obviously can easily adapt to any morphology once the surface energy situation has slightly changed. The elongated morphology probably suggests the polar *c*-axis as the long axis. However, the fact that these structures are tilted towards the surface with differing tilt angles indicates that the initial heterogeneous nucleation event of those superstructures occurs on glass along a variety of different calcite faces. This is in contrast to the defined nucleation faces observed on self assembled monolayers.[60] The developed facetting of these mesocrystals combined with pronounced curvature indicates that the mesocrystals are formed according to a self organization program which is controlled by the surface tension and interaction of the nanoparticle building units.

In the present context, we can only speculate about the reasons for the observed family-type polymorphism of mesocrystals driven by nucleation. One reason might be the well defined, monodisperse nature of the peptide binding motif which can potentially lead to regular adsorption patterns of functionality onto the glass slide being suitable for such regular, large size, high index nucleation patterns.

A further increase of polymer modifier concentration to 0.5 g/L gives again a completely altered crystallization scenario. Here, rounded truncated trigonal structures are found. Heterogeneous nucleation leads to single species which obviously nucleate again from the {001}-face, as deduced from the fact that {001} are the only triangular/hexagonal faces of calcite. Homogeneous nucleation interestingly results in the same species, which are then twinned into a staggered trigonal-bipyramidal morphology, i.e. a "diabolo" (both species are shown in **Fig. 5**(a)). Due to symmetry reasons, the assembly of nanoparticles presumably starts from a

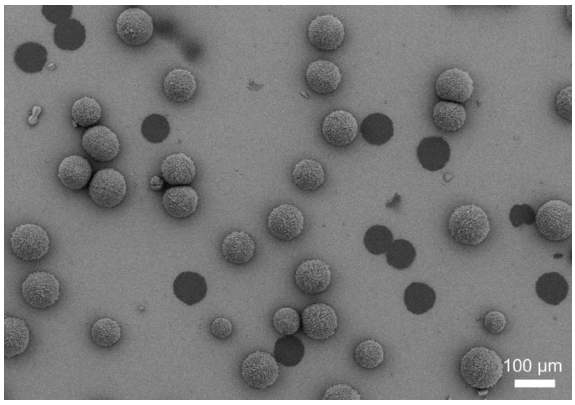

Fig. 6. Typical SEM image of calcite mesocrystals obtained on a glass slip by the gas diffusion reaction after 1 d at 10 mmol/L Ca^{2+} and [PEO-b- P(L-Asp)$_{20}$] = 0.75 g/L. The dark spots indicate positions of detached hemispheres.

primary, central hexagon exposing the two {001} faces and then proceeds along *c*-direction with a distinct opening angle. This speaks for cooperative field effects throughout nanoparticle alignment, i.e. the intermediate nanoparticle species supporting the growth of the structure are attracted by the two "poles" of the structure.

Increase of polymer concentration beyond this value leaves this structure set-up as such, but only increases the opening angle and allows the cones to close to hemispheres, as found for polymer concentrations of 0.75 g/L (Fig. 5(b)) and 1.0 g/L. These hemispheres have about the same size of approximately 100 μm like the triangular structures in Fig. 5(a). The fine surface texture

of these hemispheres is also highly ordered and composed of partly self-similar, interlaced *c*-directional corners of calcite, as suggested by the triangular base of the outgrowths. The hemispheres are heterogeneously nucleated, rather defined in size and only loosely attached to the glass surface as can be seen from many detached hemispheres (**Fig. 6**.)

This motif indeed continues the structures of Fig. 4(a) (0.1 g/L) and Figs. 5(a) and (b) (0.5 g/L resp. 0.75 g/L): with increasing polymer concentration the spontaneous curvature of the structures (or the tilt angle between two neighbouring crystals) is increased, and a continuous transition between an unbent assembled object with translational order to a crystalline hemisphere with spherulitic texture can be adjusted by polymer concentration, only.

4. Discussion and conclusion

The most surprising fact of the present experiments is the unexpected high efficiency of the presented PEO–D_{20} polymer. Already at concentration of 10^{-3} g/L or in the ppm region, efficient change of the nucleation mechanism is found, turning a "regular" default calcite crystal into a mesocrystal with surface roughness and developed texture. This is due to a very good nucleation efficiency of this polymer, as indicated by a quantitative titration assay. Calculating from the determined $CaCO_3$ concentrations and a primary particle size of 50 nm (assumed spherical) for simplicity, we end up with an efficient control of such a particle by about 200–500 polymers, only. This is one polymer for 40 nm^2 of particle in the low polymer limit, a very illustrative number for the high polymer efficiency. Interestingly, this number is very similar to the corresponding emulsion stabilization efficiency of a similar peptide block copolymer in emulsion polymerization.[61)]

However, for calcite, this low concentration is not enough to effectively stabilize amorphous intermediates, and direct crystallization as found. For a tenfold higher polymer concentration or 10 ppm, the corresponding stabilization number goes down to 4 nm^2/polymer, and effective temporal stabilization of a PILP phase is found, presumably in addition to the nucleation efficiency. This is very reasonable, as 20 Aspartate units are about the number to cover 4 nm^2.

Interestingly, we also find for this concentration pronounced heterogeneous nucleation via the *c*-plane, which is a charged plane. Its stabilization and exposure relies on charge compensation by the oppositely charged polymer. {001} nucleation therefore starts to set-in at about the point where there is enough polymer to compensate for the charges of the exposed {001} faces. This is again an indication for the very high effectivity of this unusual crystal growth modifier: in fact most polymer molecules must be actively involved in the process.

With polymer concentration increasing further, the found mesoscale structures more and more deviate from the expectations of an ordinary crystal, and we assume that the onset of splay and missing translational order can be discussed very similar to the case of the polyelectrolyte controlled $CaCO_3$–crystallization.[43),44)] In these examples, more polymer enables stronger inner dipoles in the primary constituting nanocrystals, first controlling the stacking and assembly in a long range fashion, then later - above a critical value of collective dipole strength- forming dumbbell–like and spherical structures. All these systems, including the present one, show the joint feature to change from regular packing of nanocrystals in c-direction to a splayed dipolar arrangement of primary nanoparticles.

Nevertheless, due to the multiple roles of polymers involved in crystallization processes,[47)] every polymer/mineral couple shows very specific structural features to be discovered, and in most cases a surprising and unexpected beauty of the as formed structures is revealed. This makes this field very attractive from an aesthetic perspective, but also relevant for nanomaterials design. Further examinations on mesocrystals will certainly reveal additional mechanisms of nanocrystal self assembly and architectural opportunities towards these fascinating colloidal superstructures.

Acknowledgement We thank the Max-Planck Society for financial support and a fellowship for T.X.W. Dr. Ruiqi Song is acknowledged for SEM images.

References

1) R. L. Penn and J. F. Banfield, *Geochim. Cosmochim. Acta*, 63, 1549 (1999).
2) J. F. Banfield, S. A. Welch, H. Z. Zhang, T. T. Ebert and R. L. Penn, *Science*, 289, 751 (2000).
3) M. Niederberger and H. Cölfen, *Phys. Chem. Chem. Phys.*, 8, 3271 (2006).
4) H. Cölfen and M. Antonietti, *Angew. Chem. Int. Ed.*, 44, 5576 (2005).
5) H. Cölfen and M. Antonietti, "Mesocrystals and Non Classical Crystallization," John Wiley & Sons (2008).
6) A. N. Kulak, P. Iddon, Y. T. Li, S. P. Armes, H. Cölfen, O. Paris, R. M. Wilson and F. C. Meldrum, *J. Am. Chem. Soc.*, 129, 3729 (2007).
7) J. X. Fang, B. J. Ding and X. P. Song, *Cryst. Growth Des.*, 8, 3616 (2008).
8) D. Schwahn, Y. R. Ma and H. Cölfen, *J. Phys. Chem. C*, 111, 3224 (2007).
9) J. X. Fang, B. J. Ding, X. P. Song and Y. Han, *Appl. Phys. Lett.*, 92, 3 (2008).
10) H. Imai, "Biomineralization I: Crystallization and Self-Organization Process," Ed. by K. Naka, Springer-Verlag Berlin, Berlin (2007) Vol. 270, p. 43.
11) F. C. Meldrum and H. Cölfen, *Chem. Rev.*, 108, 4332 (2008).
12) L. Zhou and P. O'Brien, *Small*, 4, 1566 (2008).
13) A. Ahniyaz, Y. Sakamoto and L. Bergström, *Proc. Nat. Acad. Sci. U.S.A.*, 104, 17570 (2007).
14) A.-W. Xu, M. Antonietti, H. Cölfen and Y.-P. Fang, *Adv. Funct. Mater.*, 16, 903 (2006).
15) J. H. Zhan, H. P. Lin and C. Y. Mou, *Adv. Mater.*, 15, 621 (2003).
16) A. W. Xu, M. Antonietti, S. H. Yu and H. Cölfen, *Adv. Mater.*, 20, 1333 (2008).
17) T. Nishimura, T. Ito, Y. Yamamoto, M. Yoshio and T. Kato, *Angewandte Chemie-Int. Edi.*, 47, 2800 (2008).
18) O. Grassman, R. B. Neder, A. Putnis and P. Löbmann, *Am. Mineral.*, 88, 647 (2003).
19) Y. Oaki and H. Imai, *Adv. Funct. Mater.*, 15, 1407 (2005).
20) B. Judat and M. Kind, *J. Colloid Interface Sci.*, 269, 341 (2004).
21) S. Wohlrab, N. Pinna, M. Antonietti and H. Cölfen, *Chem.-Eur. J.*, 11, 2903 (2005).
22) D. D. Medina and Y. Mastai, *Cryst. Growth Des.*, 8, 3646 (2008).
23) T. Vossmeyer, G. Reck, L. Katsikas, E. T. K. Haupt, B. Schulz and H. Weller, *Science*, 267, 1476 (1995).
24) E. V. Shevchenko, D. V. Talapin, A. L. Rogach, A. Kornowski, M. Haase and H. Weller, *J. Am. Chem. Soc.*, 124, 11480 (2002).
25) M. T. Buscaglia, V. Buscaglia, C. Bottino, M. Viviani, R. Fournier, M. Sennour, S. Presto, R. Marazza and P. Nanni, *Cryst. Growth Des.*, 8, 3847 (2008).
26) T. Lee and C. W. Zhang, *Pharm. Res.*, 25, 1563 (2008).

27) P. M. Rorvik, A. Almli, A. T. J. van Helvoort, R. Holmestad, T. Tybell, T. Grande and M. A. Einarsrud, *Nanotech.*, 19, 6 (2008).
28) Z. H. Li, A. Gessner, J. P. Richters, J. Kalden, T. Voss, C. Kubel and A. Taubert, *Adv. Mater.*, 20, 1279 (2008).
29) M. S. Mo, S. H. Lim, Y. W. Mai, R. K. Zheng and S. P. Ringer, *Adv. Mater.*, 20, 339 (2008).
30) L. Zhou, W. Z. Wang and H. L. Xu, *Cryst. Growth Des.*, 8, 728 (2008).
31) L. Zhou, D. Smyth-Boyle and P. O'Brien, *J. Am. Chem. Soc.*, 130, 1309 (2008).
32) Y. Oaki and H. Imai, *Small*, 2, 66 (2006).
33) Y. Oaki, A. Kotachi, T. Miura and H. Imai, *Adv. Funct. Mater.*, 16, 1633 (2006).
34) I. Sethmann, A. Putnis, O. Grassmann and P. Löbmann, *Am. Mineral.*, 90, 1213 (2005).
35) I. Sethmann, R. Hinrichs, G. Wörheide and A. Putnis, *J. Inorg. Biochem.*, 100, 88 (2006).
36) Y. Dauphin, *Palaontolog. Z.*, 75, 113 (2001).
37) X. D. Li, W. C. Chang, Y. J. Chao, R. Z. Wang and M. Chang, *Nano Lett.*, 4, 613 (2004).
38) Y. Oaki and H. Imai, *Angew. Chem. Int. Edi.*, 44, 6571 (2005).
39) M. Rousseau, E. Lopez, P. Stempfle, M. Brendle, L. Franke, A. Guette, R. Naslain and X. Bourrat, *Biomaterials*, 26, 6254 (2005).
40) M. Rousseau, E. Lopez, A. Coute, G. Mascarel, D. C. Smith, R. Naslain and X. Bourrat, *J. Struct. Biol.*, 149, 149 (2005).
41) Y. Dauphin, *J. Biol. Chem.*, 278, 15168 (2003).
42) G. Wulff, *Zeitschrift Fur Krystallographie Und Mineralogie*, 34, 449 (1901).
43) T. X. Wang, H. Cölfen and M. Antonietti, *J. Am. Chem. Soc.*, 127, 3246 (2005).
44) T. X. Wang, M. Antonietti and H. Cölfen, *Chem.-Eur. J.*, 12, 5722 (2006).
45) M. G. Page and H. Cölfen, *Cryst. Growth Des.*, 6, 1915 (2006).
46) A. Neira-Carrillo, D. F. Acevedo, M. C. Miras, C. A. Barbero, D. Gebauer, H. Cölfen and J. L. Arias, *Langmuir*, 24, 12496 (2008).
47) D. Gebauer, H. Cölfen, A. Verch and M. Antonietti, *Adv. Mater.*, 21, 435 (2009).
48) J. H. Adair and E. Suvaci, *Current Opinion in Colloid & Interface Science*, 5, 160 (2000).
49) H. Cölfen, *Macromol. Rapid Commun.*, 22, 219 (2001).
50) B. A. Gotliv, N. Kessler, J. L. Sumerel, D. E. Morse, N. Tuross, L. Addadi and S. Weiner, *Chembiochem*, 6, 304 (2005).
51) S. Collino, I. W. Kim and J. S. Evans, *Cryst. Growth Des.*, 6, 839 (2006).
52) M. G. Page, N. Nassif, H. G. Börner, M. Antonietti and H. Cölfen, *Cryst. Growth Des.*, 8, 1792 (2008).
53) Y. R. Ma, H. G. Börner, J. Hartmann and H. Cölfen, *Chem.-Eur. J.*, 12, 7882 (2006).
54) J. F. Lutz and H. G. Börner, *Prog. Poly. Sci.*, 33, 1 (2008).
55) D. Eckhardt, M. Groenewolt, E. Krause and H. G. Börner, *Chem. Commun.*, 2814 (2005).
56) D. Gebauer, A. Völkel and H. Cölfen, *Science*, 322, 1819 (2008).
57) R. Azoury, A. D. Randolph, G. W. Drach, S. Perlberg, N. Garti and S. Sarig, *J. Cryst. Growth*, 64, 389 (1983).
58) C. G. Sinn, R. Dimova and M. Antonietti, *Macromolecules*, 37, 3444 (2004).
59) L. B. Gower and D. J. Odom, *J. Cryst. Growth*, 210, 719 (2000).
60) J. Aizenberg, A. J. Black and G. M. Whitesides, *Nature*, 398, 495 (1999).
61) H. Kukula, H. Schlaad and K. Tauer, *Macromolecules*, 35, 2538 (2002).

Helmut Cölfen studied Chemistry at Duisburg University, Germany and completed his Ph.D. on Analytical Ultracentrifugation of gels in 1993 (Prof. Werner Borchard). He then went to the National Centre for Macromolecular Hydrodynamics at the University of Nottingham, England to work with Prof. Stephen Harding on the solution characterisation of complex biopolymers and their interactions and superstructures. 1995 he joined the Max-Planck-Institute of Colloids and Interfaces where he is currently leading the projects "Biomimetic Mineralisation" and "Fractionating Colloid Analytics" in Prof. Markus Antonietti's group. Since his habilitation in 2001, he is senior scientist and head of the analytical service in the colloid chemistry department and became private docent at the university of Potsdam (since 2004).

Markus Antonietti has studied Chemistry in Mainz and did his doctorate with Hans Sillescu. His habilitation about nanostructured polymergels in 1990 filled him with enthusiasm for complex materials. After his professorship for Chemistry at the University of Marburg he was appointed director for the department of Colloid Chemistry at the Max Planck Institute of Colloids and Interfaces in 1993. Markus Antonietti's contributions to the chemical community comprise manifold things, but first of all he is interested in the creativity in research. He loves to share and impart this passion. He likes cooking with his family and loud music.